Generic features of late-stage crystal growth

Fong Liu and Nigel Goldenfeld
Department of Physics and Materials Research Laboratory, University of Illinois at Urbana-Champaign, 1110 West Green Street, Urbana, Illinois 61801
(Received 5 March 1990)

A cell dynamical system model, which realistically incorporates diffusion, is developed to study various aspects of late-stage crystal growth. The algorithm is computationally efficient, allowing the development of complex spatial structures to be studied, and is motivated by renormalization group considerations. We establish the existence of an asymptotic dense branching morphology and relate it to diffusion-limited aggregation. Our findings indicate that the radius of a dense-branching structure grows linearly with time, despite being diffusion controlled, in agreement with experimental observations of the growth of spherulites. A clear morphological transition from kinetic-effect-dominated growth to surface-tension-dominated growth is observed, marked by a difference in the way growth velocity scales with undercooling. We also study the evolution of interfacial instability and find scaling behavior for the interface power spectra, indicating the nonlinear selection of a unique length scale, insensitive to short length-scale fluctuations.

I. INTRODUCTION

Dendritic crystal growth[1] is well-known example of pattern formation in nonequilibrium systems, where simple mechanisms may generate complex structures due to intrinsic dynamic instabilities. It is closely related to other pattern formation phenomena such as viscous fingering,[2] electrochemical deposition,[3] as well as diffusion-limited aggregation (DLA).[4] Much effort has been devoted to the understanding of the dynamics of both pattern formation and selection in these systems.

The canonical example is crystal growth from a supercooled melt, where the primary physical process is diffusion of the latent heat released while the liquid solidifies. The motion of the liquid-solid interface is controlled by the rate of this latent heat diffusion. The resulting crystal usually takes the form of a branching dendritic structure with appropriate crystallographic symmetry. The frequent branching events and thus the complex interface geometry, result from the diffusive instability attributed to Mullins and Sekerka.[5] Close inspection of the single-crystal dendritic structure reveals that it is composed of nearly parabolic tips decorated by sidebranches.

Recent studies of dendritic growth[1] have focused on steady-state properties, and in particular, on understanding the dynamical selection of the parabolic needle crystal and its stability. It is now believed that surface tension is a singular perturbation of the continuous family of steady-state uniformly translating crystals (needle crystals) that exist in its absence. Furthermore, the crucial role of crystalline anisotrophy has been elucidated;[6] dendrites only form if there is anisotropy present in the growth process. With both surface tension and anisotropy present, a unique, stable needle crystal is selected.[7]

Despite the progress made in steady-state problems, the interesting regime of time-dependent nonlinear growth has never been fully explored, in most part due to the numerical difficulty in solving the formidable moving boundary problem. Important questions remain to be answered by time-dependent nonlinear studies. One of the questions concerns the origin of sidebranching: whether sidebranches are caused by noise or some deterministic mechanisms. Although it is generally believed that the selected needle crystal is linearly stable,[8] with continuous noise being responsible for the sidebranches,[9,10] it is conceivable that a satisfactory understanding of sidebranching may come only from nonlinear analysis. Furthermore, the validity and effects of the quasistatic approximation must be critically examined. This approximation essentially replaces the diffusion equation with Laplace's equation; when this is done in the laboratory frame, this amounts to taking the infinite diffusion length limit. As we shall see, a finite diffusion length is responsible for the selection of a constant length scale of the growth structure in the late stage of growth, whilst the quasistatic approximation may generate a length scale that grows in time. Another question regards the existence of the dense-branching morphology.[11]

Ubiquitous as it is, dendritic growth along well-defined crystallographic directions does not seem to be the only mode of growth in solidification. It is frequently found that a compact branching structure with stable radial envelope occurs, for example, in the melt growth of a wide class of polymeric and other materials.[12,13] Ben-Jacob *et al.* referred to this structure as the dense-branching morphology (DBM) and proposed that it is an alternative mode for diffusion-controlled growth.[14] They also regarded the radial fingering patterns in Hele-Shaw cells and patterns in electrochemical depositions as examples of this morphology.[3] However, it is not clear[11] whether or not the DBM, as identified by Ben-Jacob *et al.*, truly exists, whether or not it is only a transient to DLA structure, and whether or not it can be explained merely on grounds of diffusion-controlled growth.

In this paper, we investigate the time-dependent

crystal-growth process using an effective cell dynamical scheme (CDS) model.[15] Lacking a feasible analytic method, this model provides a useful alternative to solving the partial differential equations. Our CDS model is not obtained from a discretization of partial differential equations; although it does reduce to them in the continuum limit, it contains the essential physics of crystal growth. We hypothesize that there exist universal scaling phenomena in the crystal-growth process, which are exhibited by a class of dynamical systems regardless of the precise details of each system. In this sense, our model is, we believe, in the same universality class as genuine crystal growth; accordingly, we expect that qualitative features and scaling results from our simulations should be experimentally testable. The CDS method was first proposed by Oono and Puri,[15] and has been successfully applied to the study of universal features of phase separation and fluid dynamics.[15,16]

We concentrate on the late-stage morphological aspects of crystal growth. A detailed description of the model is given in Sec. II. This model vividly simulates the complete time-dependent crystal-growth process, recovering a variety of different growth morphologies observable in real experiments. In Sec. III, we exhibit a morphological transition from a crystal growing along the axial direction to one growing along the diagonal direction, as the degree of undercooling is varied, as has previously been reported in studies of the boundary-layer model of solidification.[17] In Secs. IV and V, we present evidence showing that the asymptotic growth structure under weak anisotropy is a DBM with fractal dimension 2, rather than a DLA-like structure. We thus identify the DBM as another growth mode beside dendritic growth, which accounts naturally for the widespread occurrence of spherulites.[12,13] In particular, the radius R is observed to depend linearly on time t; this scaling law has often been interpreted as implying that spherulitic growth is not a consequence of diffusion-controlled dynamics. Our simulation conclusively demonstrates that $R \sim t$ can follow from diffusion-controlled growth, as suggested earlier.[12] Studies on the power spectra of the interfacial instability in Sec. VI indicate the nonlinear selection of a unique length scale for the growing solid-liquid interface. Qualitatively similar findings have been reported in other studies of interfacial growth, which have not been able to attain such late stages in the evolution of the interface.[18,19] Finally, the implications of our simulations on the origin of sidebranching are also discussed.

II. CELL DYNAMICAL SYSTEM MODEL OF SOLIDIFICATION

The process of crystal growth from supercooled liquid can be described by the continuum model:[20]

$$\partial_t u = D\nabla^2 u \ , \tag{2.1}$$

$$v_n = -D\nabla u \cdot \mathbf{n}\Big|_{\text{sol}}^{\text{liq}} , \tag{2.2}$$

$$u_s = \Delta - d_0(\theta)\kappa - \beta(\theta)v_n \ . \tag{2.3}$$

Here $u(\mathbf{x},t)$ is the dimensionless temperature field, D is the diffusion constant, v_n is the velocity of the interface along normal $\mathbf{n}$, u_s is the temperature at the interface, Δ is the dimensionless undercooling that acts as the driving force for crystal growth, $d_0(\theta)$ is the anisotropic capillary length, κ the curvature of the interface, and $\beta(\theta)$ is a kinetic coefficient. The angle θ is the angle between $\mathbf{n}$ and a crystallographic direction. Temperatures are expressed as dimensionless variables by the relation $u(x,t)=[T(x,t)-T_\infty]/(L/C_p)$, where L is latent heat and C is the heat capacity of the liquid at constant pressure. Boundary condition (2.3) is a modification of the Gibbs-Thomson condition, in which the second term on the right-hand side (rhs) accounts for the equilibrium surface tension effect, while the term $-\beta v_n$ represents the linear interfacial kinetics, reflecting the fact that a moving interface is slightly perturbed from local equilibrium.

In our lattice model, crystal growth occurs on two-dimensional square lattices, easily extendable to a hexagonal lattice or to three-dimensions. Lattice sites are labeled i and assigned two variables: a continuous temperature u_i^n and a binary-valued phase field $\phi_i^n \in \{0,1\}$ with n denoting the discrete time. $\phi_i = 1(0)$ if site i is solid (liquid). The growth process corresponds to the updating of space $(u_i^n, \phi_i^n) \rightarrow (u_i^{n+1}, \phi_i^{n+1})$ according to the following rules:[21]

(a) At time step n, all perimeter sites defined as liquid sites ($\phi_i = 0$) with at least one *nearest* solid neighbor are identified. Crystallization occurs only on these perimeter sites. Remelting from solid to liquid is forbidden.

(b) Determine if perimeter site i is to crystallize. The condition for crystallization is

$$u_i \le \Delta[1+\delta\eta(i,n)] + \lambda \left[\sum_{j \in \text{neighbors}} \omega_j \phi_j - 6 \right] , \tag{2.4}$$

where j is summed over neighbors of i with weights $\omega_j = 2$ for nearest neighbors and $\omega_j = 1$ for next-nearest neighbors; $\eta(i,n)$ is a random number uniformly distributed in $[-1,1]$ and $0 \le \delta < 1$ is the noise amplitude. Condition (2.4), coupling the temperature field and phase field together, corresponds to the Gibbs-Thomson boundary condition (2.3). This can be recognized by noticing that the term $-(\sum_j \omega_j \phi_j - 6)$ approximates the local interface curvature just as in the DLA simulations,[22] where interface curvature is calculated by counting the number of solid particles in a box centered at the interface. Hence, the parameter λ plays the role of capillary length.

Our model is deterministic by construction, in contrast to DLA-type simulations. However, randomness or noise can be rather conveniently incorporated if desired, either by choosing a random initial seed or by adding a stochastic term to the undercooling; this is the purpose of the η term in equation (2.4). The latter mimics persistent noise in real crystal-growth experiments.

(c) Let all perimeter sites that satisfy condition (2.4) solidify simultaneously, and add latent heat l_a to those sites by increasing the local temperature:

$$u_i \rightarrow u_i + l_a \ . \tag{2.5}$$

(d) Finally the temperature field is relaxed through

diffusion, according to an explicit finite difference scheme:

$$u_i = u_i + \frac{D}{m}(\langle u \rangle - u_i) , \tag{2.6}$$

where D is the diffusion constant, m is an integer, and $\langle\ \rangle$ denotes an average over nearest neighbors (NN) and next-nearest neighbors (NNN) in the same spirit as in step (b):

$$\langle u \rangle = \tfrac{1}{6} \sum_{j \in \mathrm{NN}} u_j + \tfrac{1}{12} \sum_{j \in \mathrm{NNN}} u_j . \tag{2.7}$$

Here we consider the symmetric model so that the diffusion constants in liquid and solid are identical. Physically, temperature field relaxation occurs more slowly than the relaxation of the phase field, so (2.6) is repeated $m > 1$ times. The continuum limit (2.1) is recovered as $m \gg 1$.

Note that the effect of crystalline anisotropy is inevitably contained in (2.4) as a result of the underlying square lattice and discreteness of the phase field. A more subtle observation is the implicit presence of the nonequilibrium effect of interfacial kinetics mentioned above. The nonequilibrium kinetic effect,[23] in essence, reflects the fact that the interfacial attachments of the crystallizing atoms or molecules occur within a finite characteristic time, rather than instantaneously. Now observe the inequality $\leq$ in condition (2.4). It implies that a perimeter site may be "under" cooled below the threshold temperature needed for crystallization. This is equivalent to the statement that a qualified perimeter site has to wait for a certain relaxation time before it can crystalize. Hence an effective kinetic effect is present. Such a nonequilibrium kinetic effect is, in general, more complicated than the oversimplified linear form βv_n in equation (2.3). Unfortunately, we have little quantitative control of either the anisotropy strength or of the extent of kinetic effects, and so we assume that these dependences are implicitly contained in the undercooling Δ. This difficulty hinders direct quantitative comparisons between simulations and the steady-state analytic theory.[1] In fact, we do not expect agreement with analytic theory in general because of the dependence of the anisotropy strength and the kinetic coefficient on undercooling. This is clear in our model and, presumably may also be true for experiments.

The parameters D, m, λ, and l_a merely determine the length, time, and temperature scales of the simulation and may be set to convenient values and kept fixed. The undercooling Δ is the control parameter that we may adjust. For the sake of numerical efficiency, all arithmetic operations are performed in integers rather than floating-point numbers. Our algorithm is extremely fast and well suited for massively parallel processors such as the Connection Machine. The simulations reported here were performed on VAX 780 and MicroVax computers, typically taking of order 2 h, CPU to generate the cluster of 85 171 particles in Fig. 2(b).

III. MORPHOLOGICAL TRANSITIONS

We first simulate crystal growth from the center of a square lattice of size as large as 1400×1400 sites. By varying the control parameters, the model generates a wide variety of growth morphologies that have been observed in real crystal-growth experiments, as shown in Figs. 1 and 2. The evolution of the interface as well as the temperature fields can be monitored over the complete growth process to the very late stages. Growth initiates from a 5×5 seed with half of its sites randomly occupied. The initial temperature is zero everywhere except on solid sites, where is has the value Δ. In Figs. 1 and 2 we show some typical crystal growth patterns. Figure 2 shows clusters grown under different undercooling, with all the other parameters kept constant. Gray levels in the picture reflect the temperature scale of the diffusion field.

We have invariably observed that at relatively large undercoolings $\Delta > 0.125$, the crystal patterns are dense dendritic structures growing preferentially along the symmetry axes [Fig. 2(a)]. In contrast, for small undercoolings $\Delta < 0.125$, we observe a less frequently branching dendrite, growing dominantly along diagonals, as illustrated in Figs. 2(c) and 2(d). There is an intermediate regime of almost isotropic growth, shown in Fig. 2(b), where the branching or tip-splitting events occur in a seemingly random manner. This morphology will be identified as the dense-branching morphology (DBM),[14] to be discussed later.

This transition of growth direction can be readily compared with observations of dendritic growth of NH_4Cl crystals in an aqueous solution.[24] There, a transition from dendrites oriented along the $\langle 100 \rangle$ direction to dendrites oriented along the $\langle 111 \rangle$ direction is found as the degree of supersaturation is increased, accompanied by an intermediate regime where nonstationary dendritic tips split periodically. A transition in growth direction in experiments on Hele-Shaw cells with a grid imposed on one of the plates has also been reported.[17]

In addition to the explicit demonstration of Fig. 2, the morphological transition also manifests itself in the veloc-

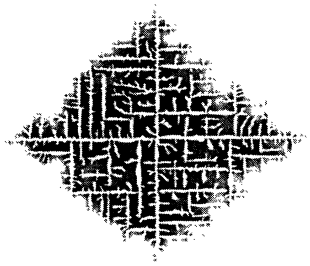

FIG. 1. Dendritic crystal grown with the lattice model. Grey levels represent temperature value of the diffusion field. Parameters are $D = 4.0$, $m = 5$, $\lambda = 0.015$, $l_a = 1$, $\Delta = 0.195$, and $\delta = 0.1$.

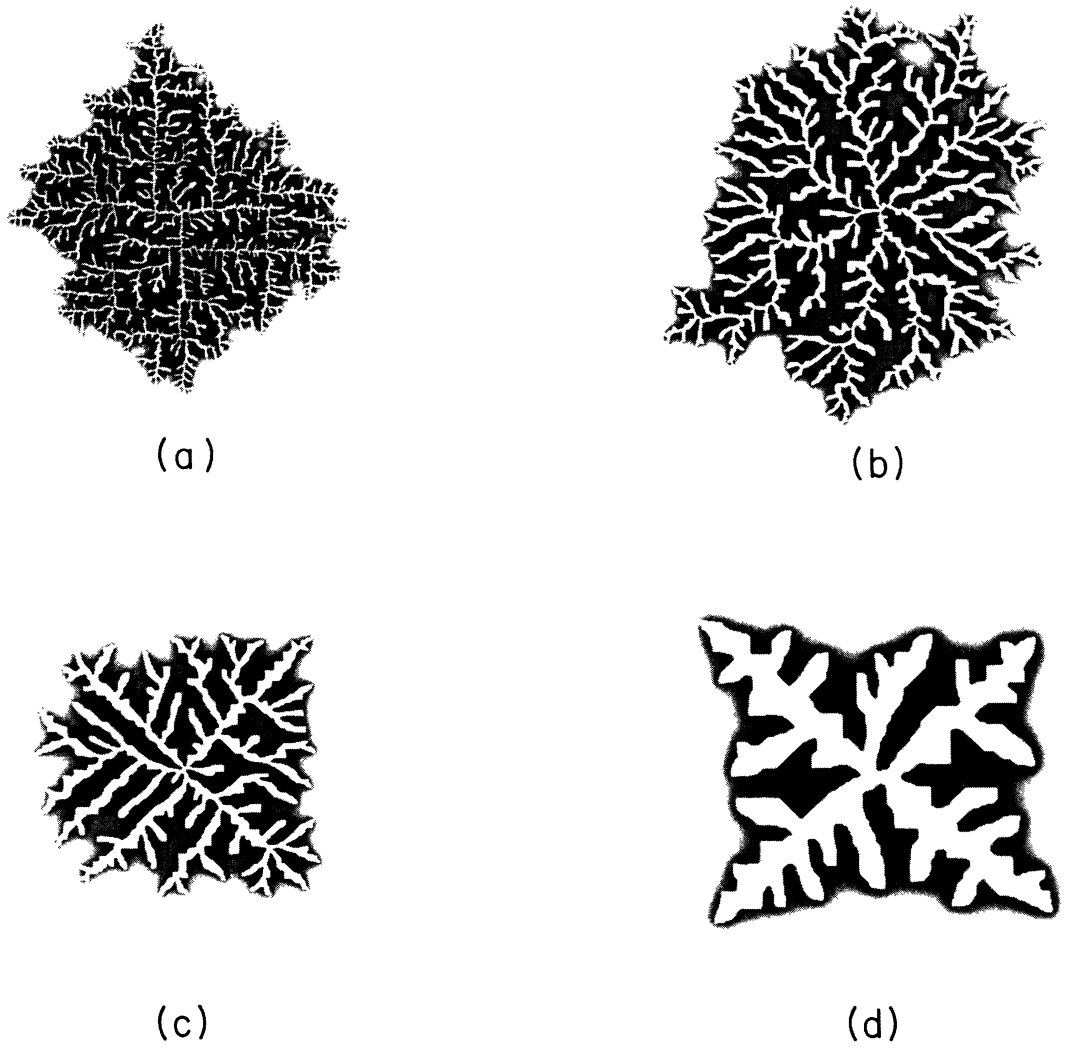

FIG. 2. The morphological transition from axial to diagonal growth. All crystals are grown at $\lambda=0.01$, $\delta=0.2$, but with different Δ. (a) $\Delta=0.15$, the cluster has 85 171 solid particles; (b) $\Delta=0.125$, with 144 522 particles; (c) $\Delta=0.1$, 94 072 particles; and (d) $\Delta=0.05$, 47 305 particles. The scale of picture (d) has been doubled.

ity plot as a function of undercooling. We define the growth velocity $v=dR/dt$, where R is the rms radius of the crystal aggregate. In all simulations, R shows linear growth $R\sim t$ at sufficiently late stages of the growth, after an initial transient of $R\sim t^{1/2}$ behavior, as shown in Fig. 3. This linear growth behavior is independent of the amount of noise in the simulation, and is also robust to variations of the crystalline anisotropy.

Figure 4 displays v as a function of undercooling Δ, averaged over 15 clusters grown with random initial conditions. At $\Delta\sim 0.125$, where the morphological transition occurs, there is an abrupt change of dependence of v on Δ. The $v(\Delta)$ dependence is fitted with *approximate* power laws in the inset of Fig. 3. We obtain $v\sim\Delta^{5.5}$ at large Δ and $v\sim\Delta^{1.3}$ at small Δ. The change of velocity scaling seems to be a common feature in several systems exhibiting morphological transitions. In electrodeposition, it is observed[17] (see Fig. 4 of Ref. 17) that the interfacial growth velocity follows $v\sim V^{3.61}$ at large voltage V, changing to $v\sim V^{0.64}$ at small voltages. Steeper changes, even jumps in velocity scaling were reported in Chan *et al.*'s NH_4Cl crystal-growth experiments.[24]

The morphological transition observed in crystal growth and Hele-Shaw cells[17,14] is due to the fact that surface tension and kinetic anisotropies act in different directions. At low driving force, the interface moves slowly, relaxing through energetics considerations, which favor a diagonal orientation so as to minimize the interfacial free energy. At higher driving force, however, the interfacial kinetics effect gradually dominates the growth in axial direction. In recent studies of the boundary-layer model of solidification, it is found that taking into account of the kinetic anisotropy, linear stable needle crystals grow in different directions as the undercooling is varied. There also exists a region of undercooling, where needle crystals completely lost their stability, giving way to the DBM.[25] These results are compatible with our observations here.

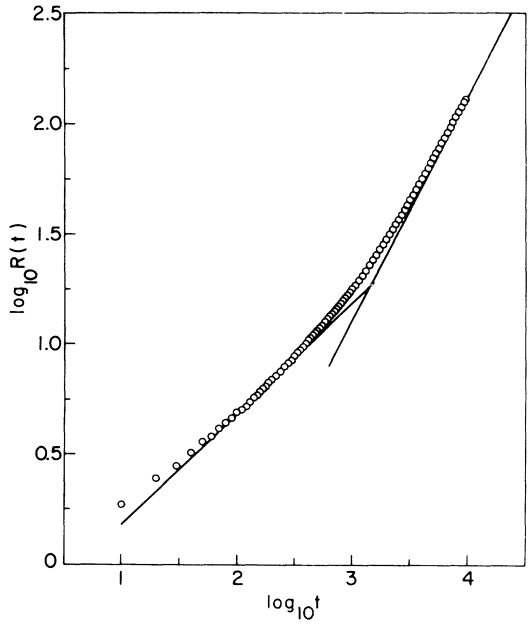

FIG. 3. Rms radius of crystal aggregate as a function of time for the crystal in Fig. 2(d). The two solid lines in the graph have slopes 0.5 and 1.0.

IV. ASYMPTOTIC GROWTH MORPHOLOGY

In this section, we investigate the long-time properties of growth and try to answer the question: what is the asymptotic ($t \to \infty$) growth structure in the absence of crystalline anisotropy? Is it a ramified DLA-like structure or the DBM—a branching structure with stable circular envelope and radial symmetry? This question has been addressed for the radial fingering patterns in Hele-Shaw cells. Ben-Jacob *et al.* suggested[14] that the fingering pattern is DLA-like at early stages and eventually becomes a DBM. This issue remains controversial and is the subject of discussion by several authors.[11] The existence and origin of DBM are not well established. The solidification system differs from a Hele-Shaw system in that the governing equation is the diffusion equation rather than Laplace's equation. It is then natural to investigate the effect of finite diffusion length (or conversely the quasistatic approximation) on the asymptotic morphology.

Scaling length and time by d_0/Δ and $d_0^2/D\Delta^3$, and the temperature by Δ respectively, we cast the continuum model (2.1) into the following form:

$$\Delta \cdot \partial u/\partial t = \nabla^2 u \ , \tag{4.1}$$

$$v_n = -\nabla u \cdot \mathbf{n} \ , \tag{4.2}$$

$$u_s = 1 - \kappa \ , \tag{4.3}$$

where we have neglected the kinetic term and considered the ideal case of the isotropic one-sided model. We now have a well-posed question regarding the asymptotic morphology of Eqs. (4.1)–(4.3), which can only depend on one parameter, namely Δ. In addition, Eqs. (4.1)–(4.3) show a formal analogy to the Laplacian radial fingering in Hele-Shaw cells under zero viscosity ratio and constant driving force, if we take the $\Delta \to 0$ limit.

The fractal dimension D_f of a radial structure is defined as $N \sim R^{D_f}$, where N is the number of solid particles within radius R. Figure 5 shows NR^{-2} versus R for the final crystal aggregate in Fig. 2(a). The structure has $D_f \sim 2.0$ since $NR^{-2} \to$ const as $R \to \infty$.

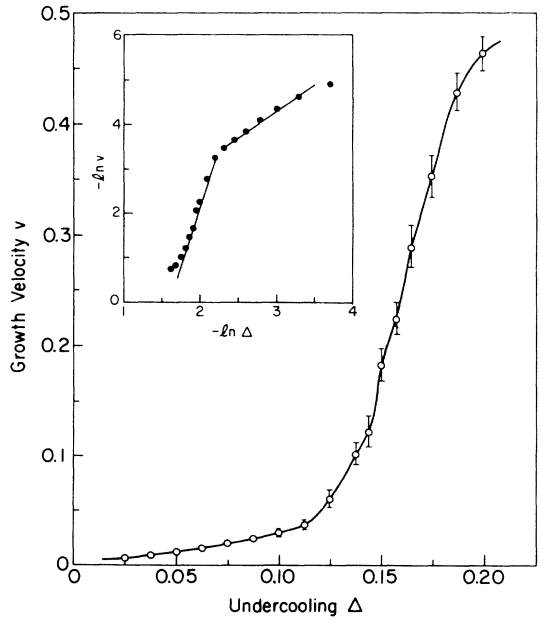

FIG. 4. Growth velocity v vs Δ with $\lambda = 0.01$ and $\delta = 0.2$. Inset is the same data plotted with log v vs log Δ.

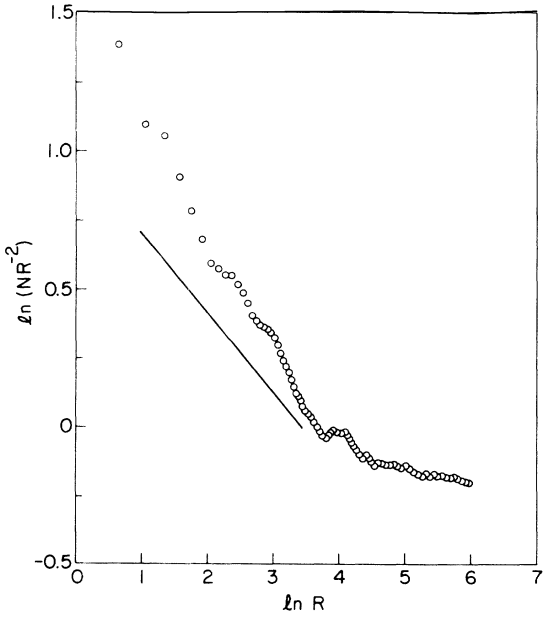

FIG. 5. Dependence of number of particles in the crystal, N, on radius R. $\Delta = 0.15$, $\lambda = 0.01$, and $\delta = 0.2$. The solid line has a slope of -0.29 to guide the eye. $NR^{-2} \to$ const as $R \to \infty$ implies $D_f = 2$. For a DLA-like structure $NR^{-2} \sim R^{-0.29}$, its plot in the figure would follow the solid line as $R \to \infty$.

It is also instructive to consider a quantity that we might call the differential fractal dimension, $\delta_f(R)$. We further regard $\delta_f(R)$ as a slow-varying function of radius R:

$$\delta_f(R)=\frac{d(\log N)}{d(\log R)} . \tag{4.4}$$

In Fig. 6, we plot $\delta_f(R)$ for undercooling $\Delta=0.15, 0.175$. Within statistical accuracy, we see that δ_f increases monotonically with R from a more or less DLA-like value 1.7 to the asymptotic DBM value $\delta_f=2$. Once $\delta_f(R)$ is independent of R over a large range of R, genuine fractal dimension can then be associated with the structure.

We have carried out simulations for $\Delta>0.12$ on 1400×1400 lattices with the same consistent result. Unfortunately, data for $\Delta\leq0.1$ are not sufficient to draw definitive conclusions, hindered by both the enhanced anisotropy effect and the slow growth. We recall that in our simulations, both anisotropy and kinetic effects are present. Therefore, strictly speaking, we are not simulating the ideal system Eqs. (4.1)–(4.3). The ideal DBM with radial envelope can only exist in the absence of anisotropy. This condition seems to be roughly satisfied at $\Delta\sim0.125$, where the competition between kinetic and surface tension anisotropies balances. The simulations strongly support the DBM as the asymptotic morphology of Eq. (4.3). Although it is conceivable that at very small undercooling, D_f could attain an asymptotic value other than 2, our data indicate that such a scenario is rather unlikely. We propose that for all nonzero $\Delta\neq0$, asymptotically $D_f=2$; only when $\Delta\to0$, can the system be thought of as the analogue of the Hele-Shaw system, where the DLA value $D_f\sim1.7$ seems to be found. This statement can be summarized by a *static* scaling hypothesis for the cluster size:

$$N(R,\Delta)=R^{D_{\rm DLA}}f(R/\xi(\Delta))=R^{D_{\rm DLA}}f(R\Delta^{\phi}) , \tag{4.5}$$

where the function f satisfies $f(x)\sim x^{2-D_{\rm DLA}}$ as $x\to+\infty$ and $f(0)=$const. $\xi(\Delta)$ is a characteristic length scale at which the structure crosses over from DLA to DBM. We assume that $\xi(\Delta)\sim\Delta^{-\phi}$ at small Δ, with ϕ being a positive exponent that can be estimated as follows. For $R\gg\xi$, $N\sim R^2\Delta^{\phi(2-D_{\rm DLA})}$; the total latent heat generated is Nl_a, causing the temperature to rise in the area πR^2. Thus we expect that $Nl_a\sim\pi R^2\cdot\Delta$, leading to $\phi=(2-D_{\rm DLA})^{-1}\sim3.45$. A scaling hypothesis of similar spirit was proposed for the Hele-Shaw flow by Lee, Coniglio, and Stanley.[11]

Another property that distinguishes the DBM from DLA is that the DBM has an approximate radial envelope moving with constant velocity. This property (i.e., $R\sim t$) was shown in Sec. III for all undercoolings. Analogous to ξ, we also expect v to follow a power law $v\sim\Delta^{\alpha}$ at small Δ, α being another positive exponent. For comparison note that $v\sim\Delta^4$ for steady-state needle crystals in two dimensions.[26] However, for the DBM, there is no reason *a priori* that guarantees that $\alpha=4$. Our data are not sufficient to accurately estimate α and ϕ due to anisotropy effects. With anisotropy, instead of getting a unique value for α, two values are obtained corresponding to different morphologies. Accurate determination of α and ϕ would be useful to understand the difference between steady-state growths and the late-stage nonlinear growths.

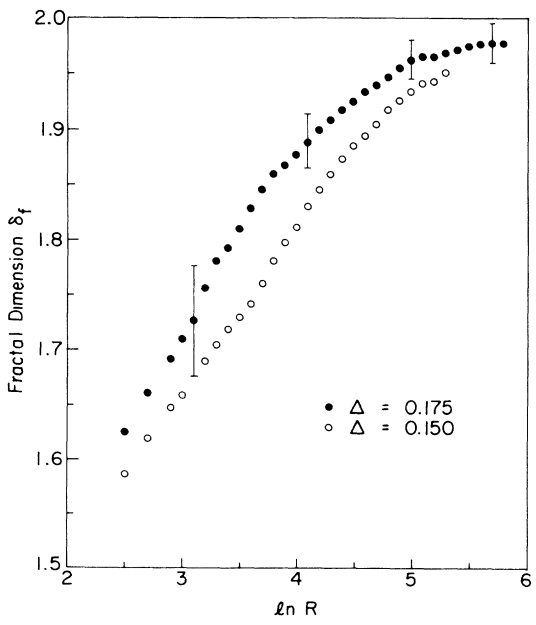

FIG. 6. Fractal dimension δ_f of the pattern varies with radius R under different undercoolings. Typical error bars are shown on a few points.

V. SPHERULITIC CRYSTALLIZATION

In most diffusion-controlled crystal-growth systems, one obtains dendritic single crystals with apparent crystalline symmetry. In certain systems, however, a more complicated structure known as the spherulite is found.[12–14] Spherulites are polycrystalline aggregates composed of a radiating array of crystalline fibers, branching successively at small, noncrystalline angles, with secondary fibers oriented slightly but appreciably different from the parent fibers. Random generation of fibers then form a space-filling structure, which is more or less radially symmetric.

Spherulites are encountered in many systems. They are frequently found in igneous rocks and glassy minerals grown from viscous and impure melts and in organic compounds that exhibit cholesteric liquid-crystal phases. Spherulitic growth is also the dominant morphology of melt grown polymers. Many of these polymeric systems also exhibit dendritic growth if the conditions for growth are altered slightly.

Previous investigators have been intrigued by the stable spherical envelope and the linear $R\sim t$ growth, but have discriminated against explanations based on diffusion-controlled growth,[27] because it is taken for granted that isotropic diffusion-controlled growth leads inevitably to $R\sim t^{1/2}$. Furthermore, circular fronts

would be destroyed by the Mullins-Sekerka instability, giving rise to dendritic growth.

The existence of the DBM at weak anisotropy offers a natural explanation for the spherulitic morphology. We have shown that although the Mullins-Sekerka instability renders the interface unstable to constant tip splitting at short length scales, the finite diffusion length is responsible for the stabilization of the interface on longer length scales, at late stages. Furthermore, $R \sim t$ follows unambiguously at late stages. The initial transient of $R \sim t^{1/2}$ also finds its counterpart in spherulitic growth.[28] The crucial common feature in the systems exhibiting spherulitic growth is the large amount of disorder (due to impurities, chain entanglements in polymers, etc.) which effectively destroys the local effect of crystalline anisotropy at the growing interface. This then leads to a destruction of the global crystallographic symmetry of the growing aggregate. We conclude that we have demonstrated explicitly that diffusion-controlled growth does lead to the qualitative and scaling features of spherulitic growth, as suggested previously.[12]

VI. INTERFACIAL STRUCTURE

Studies in the previous sections have focused on the global aspect of the crystal-growth process. In this section we analyze the dynamical evolution of interfacial instabilities from short to large length scales, in a planar geometry.

Simulations are performed in rectangular cells starting from a horizontal substrate of linear dimension L with periodic boundary condition imposed horizontally. The initial interface profile is a linear superposition of different Fourier modes with random complex coefficients. The maximum height is normalized to ~ 10 lattice units. Figure 7 demonstrates a typical growth pattern at $\Delta = 0.165$. Although we are using a different cell geometry, qualitative results obtained in previous sections such as the linear growth rate and compact growth structure are essentially unaltered.

Inspecting Fig. 7, we observe the development of interfacial instability from a short transient to a seemingly steady growth with a characteristic length scale. Interface structures can be well probed quantitatively by studying their power spectrum. In our case, we first eliminate overhangs of the interface by projecting it onto the substrate, resulting in a projected interface $h(x,t)$. The power spectrum can then be calculated:

$$P(q,t)=\frac{1}{L^2}\left|\sum_{j=1}^{L} h(x_j,t)\exp(iqx_j)\right|^2, \tag{6.1}$$

where q is the wave number.

Power spectra for $\Delta = 0.165$ from $t = 500$ through 1700 are presented in the inset of Fig. 8. Results are obtained on a $L = 600$ substrate, averaging over 20 independent runs with random initial conditions. To check whether or not the growth has indeed reached the steady state, we further scale power spectra by the interface width $w^2(t) = 1/L \sum_{j=1}^{L} [h(x_j,t) - \bar{h}]^2$, where $\bar{h}$ is the average of h over the substrate. After scaling, the power spectra for different times collapse nicely onto a single curve, as shown in Fig. 8.

Two features can be identified from the power spectrum $P(q,t)$. The first is the selection of a unique length scale from the continuum of perturbations with all possible wavelengths. This nonlinear selection mechanism, insensitive to short-wavelength fluctuations or noise, is very different from the dynamical selection principle in steady-state problems. It operates in the late stage of the growth so it cannot be understood within the linear stability analysis. The selected length scale $\bar{l}$ can be related to the average wave number $\bar{q}$ of the pattern by $\bar{l} = \pi/\bar{q}$. Here $\bar{q}(\Delta) = (\int qP(q)dq / \int P(q)dq)$, where $\bar{q}$ increases monotonically with Δ. For the interface with power

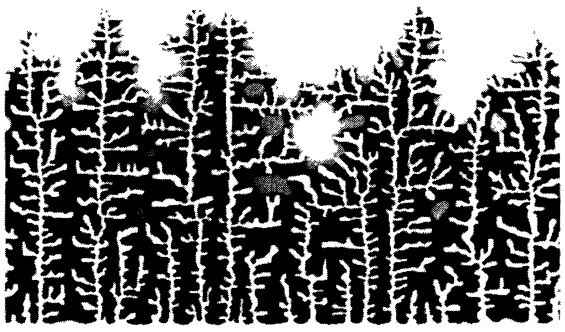

FIG. 7. Sample morphology of the growth from a planar interface. $\Delta = 0.1625$, $\lambda = 0.01$, and $\delta = 0.2$. Periodic boundary conditions are used in the horizontal direction.

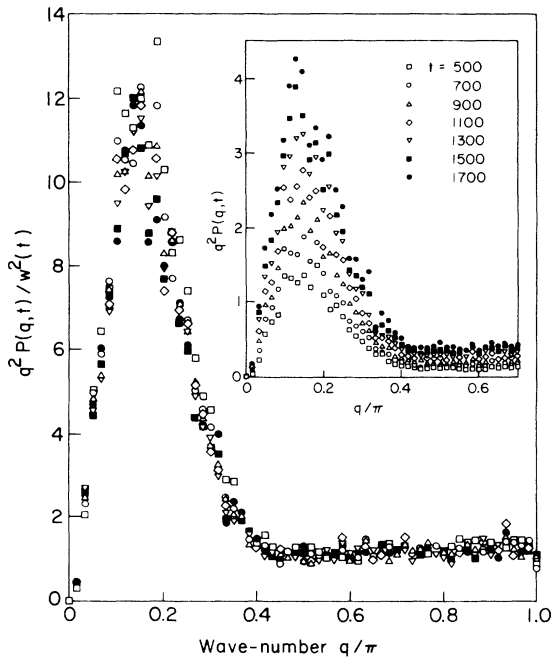

FIG. 8. Scaled power spectra $P(q,t)$ of the growing interface. Different symbols represent times from $t = 500$ to 1700. The unscaled data are shown in the inset.

spectrum Fig. 7, we find $\bar{q}=0.11$ or $\bar{l}\sim 30$ lattice units. For comparison, the fastest growing mode in the Mullins-Sekerka instability corresponds to a wavelength less than 10 lattice units.

Another feature evident from Fig. 7 is that $P(q)\sim q^{-2}$ for large q: the short-wavelength fluctuations have the spectrum of random surfaces under thermal capillary roughening. This result demonstrates that, in contrast to the case of steady-state problems, where the short-length-scale surface tension strongly affects the global shape of the needle crystal by behaving as a singular perturbation, here the short-wavelength fluctuations are irrelevant to the selection of a large length scale $\bar{l}$ during growth. Similar scaling behavior of the interface power spectra has been observed and discussed by Harris *et al.*[18] in a spin Monte Carlo study as well as by Jasnow *et al.*[19] in boundary-integral-type simulations. In the latter case, however, in contrast to finding a constant length scale as $t\to\infty$ as in Ref. 18 and in our simulations, the authors observed the characteristic length scale growing linearly in time. This result may be intrinsic to the quasistatic approximation and their constant flux boundary condition. In addition, in Ref. 19, the correlations are along the interface, not in real space.

VII. NOISE

The effect of noise is the central issue concerning the origin of dendritic sidebranching. As discussed by Martin and Goldenfeld,[10] there can be two mechanisms of sidebranching: sidebranching from a deterministic instability or from selected noise amplification. The deterministic instability in turn can be a nonlinear one, presumably involving limit cycles, or can be a simple linear instability. The noise induced sidebranching mechanism is commonly believed since the steady-state theories[1] seems to predict linearly stable free dendrites. A key distinction between the two scenarios is that the latter requires persistent noise to generate the sidebranches, whilst the former does not. Experiments have been performed toward this end but the results are not conclusive.[29]

In our deterministic simulations, we incorporate the effect of noise either through a random initial seed or by adding perturbations persistently. We find that sufficient randomness in the initial condition is enough to generate random sidebranching structures throughout the whole growth process. Noise also seems to be unimportant to the late-stage wavelength selection, as shown in the previous sections. In Fig. 9 we show a crystal grown without noise under the same conditions as those for the crystal in Fig. 2(b); one can observe that other than differences in short-length-scale randomness, the large scale structure is quite similar.

Thus our simulation suggests that, while the amplification of noise is sufficient, it is not a necessary condition for sidebranching. This conclusion is supported by a recent stability analysis of the boundary-layer model of the solidification where it is found that the competition of surface tension and kinetic anisotropy is sufficient to cause *linear* instability of the needle crystal; thus inducing sidebranchings.[25] The irrelevance of noise to the selection of late-stage growth patterns is also shown by other authors.[18,19]

VIII. SUMMARY

To summarize, we have developed a deterministic lattice model of crystal growth, which provides an efficient way of studying the generic features of the solidification process, fully treating the interface dynamics. In particular, we are able to investigate the complex structures that evolve at late stages. We find a morphological transition induces by the competition between surface and kinetics anisotropies. Under weak anisotropy, the growth structures crossover from a fractal, DLA-like, pattern at early times to the DBM, at long times.

Our study reveals that at long times, a dynamical selection principle, distinctly different from that in steady-state problems, is operating here. It is important to note the insensitivity of the nonlinear selection to short-length-scale fluctuations. This is indeed confirmed in our simulations. Noise is present either because we choose a random initial seed, or explicitly by adding randomness at each time step. We find that our results as described in the previous sections, do not depend on which of the two mechanisms is operative. We believe that in the complex crystal-growth processes, both the nonlinear and the steady-state selection principles are present. The first determines the global structure, while the latter selects the local needle crystal shapes.

Our findings also are relevant to the question of the origin of sidebranching. We find that sufficient randomness at the initial stage is enough to induce continuous sidebranching, due to nonlocal diffusion fields; a persistent noise is *not* necessary. Hence it seems that sidebranching can be attributed to the competition between the two types of anisotropy. This scenario is supported by a recent study of the boundary-layer model.[25] The competition of the two anisotropies can destroy the *linear* stability of needle crystals, thus inducing sidebranching. More work is needed in this direction before a clear picture emerges. Our preliminary conclusion on this matter

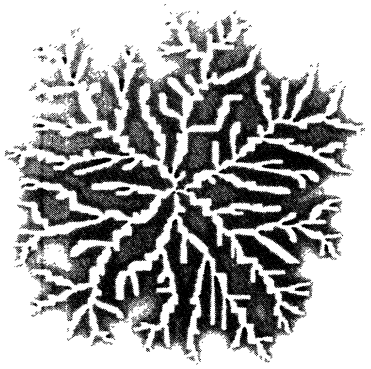

FIG. 9. Crystal grown without noise ($\delta=0$). Other parameters are identical to those of Fig. 2(b).

is that persistent noise may be a sufficient condition for sidebranching to occur, but is not a necessary condition.

In addition, we have also demonstrated the existence of several length scales in the late stages of growth, ξ, $\bar{l}$, and the diffusion length defined as $l = D/v$. It remains to see what is the relation between these lengths and to determine the exponents in the dependence of these quantities on undercooling, either through numerical or analytic studies.

ACKNOWLEDGMENTS

We are grateful to N. Packard for helpful discussions during the initiation of this project. We thank the MRL Center of Computation in the University of Illinois for the use of their facilities and J. Shannon for help with the graphics. This work is supported partially by Grant No. NSF-DMR-86-12860 and partially by Grant No. NSF-DMR-87-01393. One of us (N.D.G.) gratefully acknowledges the support of the Alfred P. Sloan Foundation.

[1]J. S. Langer, Rev. Mod. Phys. **52**, 1 (1980); D. A. Kessler, J. Koplik, and H. Levine, Adv. Phys. **37**, 225 (1988).

[2]D. Bensimon, L. P. Kadanoff, S. Liang, B. I. Shraiman, and C. Tang, Rev. Mod. Phys. **58**, 977 (1986).

[3]Y. Sawada, A. Dougherty, and J. P. Gollub, Phys. Rev. Lett. **56**, 1260 (1986); D. G. Grier, D. A. Kessler, and L. M. Sander, Phys. Rev. Lett. **59**, 2315 (1987); D. Grier, E. Ben-Jacob, R. Clarke, and L. M. Sander, *ibid.* **56**, 1264 (1986); P. Garik, D. Barkley, E. Ben-Jacob, E. Bochner, N. Broxholm, B. Miller, B. Orr, and R. Zamir, *ibid.* **62**, 2703 (1989).

[4]See *Kinetics of Aggregation and Gelation,* edited by F. Family and D. P. Landau (North-Holland, Amsterdam, 1984).

[5]W. W. Mullins and R. F. Sekerka, J. Appl. Phys. **34**, 323 (1963); **35**, 444 (1964).

[6]E. Ben-Jacob, N. Goldenfeld, J. S. Langer, and G. Schön, Phys. Rev. Lett. **51**, 1930 (1983).

[7]E. Ben-Jacob, N. Goldenfeld, B. G. Kotliar, and J. S. Langer, Phys. Rev. Lett. **53**, 2110 (1984); D. A. Kessler, J. Koplik, and H. Levine, Phys. Rev. A **31**, 1712 (1985).

[8]D. A. Kessler and H. Levine, Phys. Rev. Lett. **57**, 3069 (1986); F. Liu and N. D. Goldenfeld, Phys. Rev. A **38**, 407 (1988); D. Bensimon, P. Pelcé, and B. I. Shraiman, J. Phys. (Paris) **48**, 2081 (1987); E. A. Brener, S. V. Iordanskii, and V. I. Mel'nikov, Zh. Eksp. Teor. Fiz. **94**, 320 (1988) [Sov. Phys.—JETP **67**, 2574 (1988)].

[9]R. Pieters and J. S. Langer, Phys. Rev. Lett. **56**, 1948 (1986).

[10]O. Martin and N. D. Goldenfeld, Phys. Rev. A **35**, 1382 (1987).

[11]S. E. May and J. V. Maher, Phys. Rev. A **40**, 1723 (1989); C. Yeung and D. Jasnow, *ibid.* **41**, 891 (1990); J. Lee, A. Coniglio, and H. E. Stanley, *ibid*, **41**, 4589 (1990).

[12]See N. D. Goldenfeld, J. Cryst. Growth. **84**, 601 (1987), and references therein.

[13]D. C. Bassett, *Principles of Polymer Morphology, (Cambridge University Press, London,* 1981).

[14]E. Ben-Jacob, G. Deutscher, P. Garik, N. D. Goldenfeld, and Y. Lereah, Phys. Rev. Lett. **57**, 1903 (1986).

[15]Y. Oono and S. Puri, Phys. Rev. Lett. **58**, 836 (1987); Y. Oono and S. Puri, Phys. Rev. A **38**, 434 (1988); S. Puri and Y. Oono, *ibid.* **38**, 1542 (1988).

[16]Y. Oono and A. Shinozaki, Forma (to be published).

[17]E. Ben-Jacob, P. Garik, D. Grier, and T. Muller, Superlatt. Microstruct. **3**, 599 (1987); see also the DLA-type simulation, T. Aukrust, M. A. Novotny, D. A. Browne, and K. Kaski, Phys. Rev. A **39**, 2587 (1989).

[18]R. Harris and M. Grant (unpublished).

[19]D. Jasnow and Jorge Viñals, Phys. Rev. A **40**, 3864 (1989); and (unpublished).

[20]N. D. Goldenfeld, in *Physicochemical Hydrodynamics,* edited by M. Verlarde (Plenum, New York, 1988), p. 547.

[21]Our model is an outgrowth of that developed by N. Packard, in *Theory and Applications of Cellular Automata,* edited by S. Wolfram (World Scientific, Singapore, 1988); note that in the earlier model of Packard, the rules do not correspond to the correct boundary condition for diffusion-controlled crystal growth.

[22]T. Vicsek, Phys. Rev. Lett. **53**, 2281 (1984); and Phys. Rev. A **32**, 3084 (1985). See also L. P. Kadanoff, J. Stat. Phys. **39**, 267 (1985).

[23]J. W. Cahn, W. B. Hillig and G. W. Sears, Acta Metall **12**, 1421 (1964); see also *Crystal Growth,* edited by H. S. Peiser (Pergamon, Oxford, 1967) Secs. J and K.

[24]S-K. Chan, H. H. Reimer, and M. Kahlweit, J. Cryst. Growth. **32**, 303 (1976); *ibid.* **6**, 125 (1970).

[25]F. Liu and N. D. Goldenfeld (unpublished).

[26]B. Caroli, C. Caroli, C. Misbah, and B. Roulet, J. Phys. (Paris) **48**, 547 (1987).

[27]H. D. Keith and F. J. Padden, Jr., J. Appl. Phys., **34**, 2409 (1963).

[28]H. Tanaka and T. Nishi, Phys. Rev. Lett. **55**, 1102 (1985); Phys. Rev. A **39**, 783 (1989).

[29]A. Dougherty, P. D. Kaplan, and J. P. Gollub, Phys. Rev. Lett. **58**, 1652 (1987); A. Dougherty and J. P. Gollub, Phys. Rev. A **38**, 3043 (1988); X. W. Qian and H. Z. Cummins (unpublished).

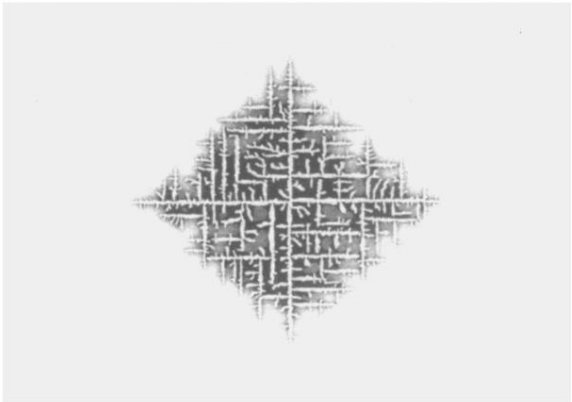

FIG. 1. Dendritic crystal grown with the lattice model. Grey levels represent temperature value of the diffusion field. Parameters are $D=4.0$, $m=5$, $\lambda=0.015$, $l_a=1$, $\Delta=0.195$, and $\delta=0.1$.

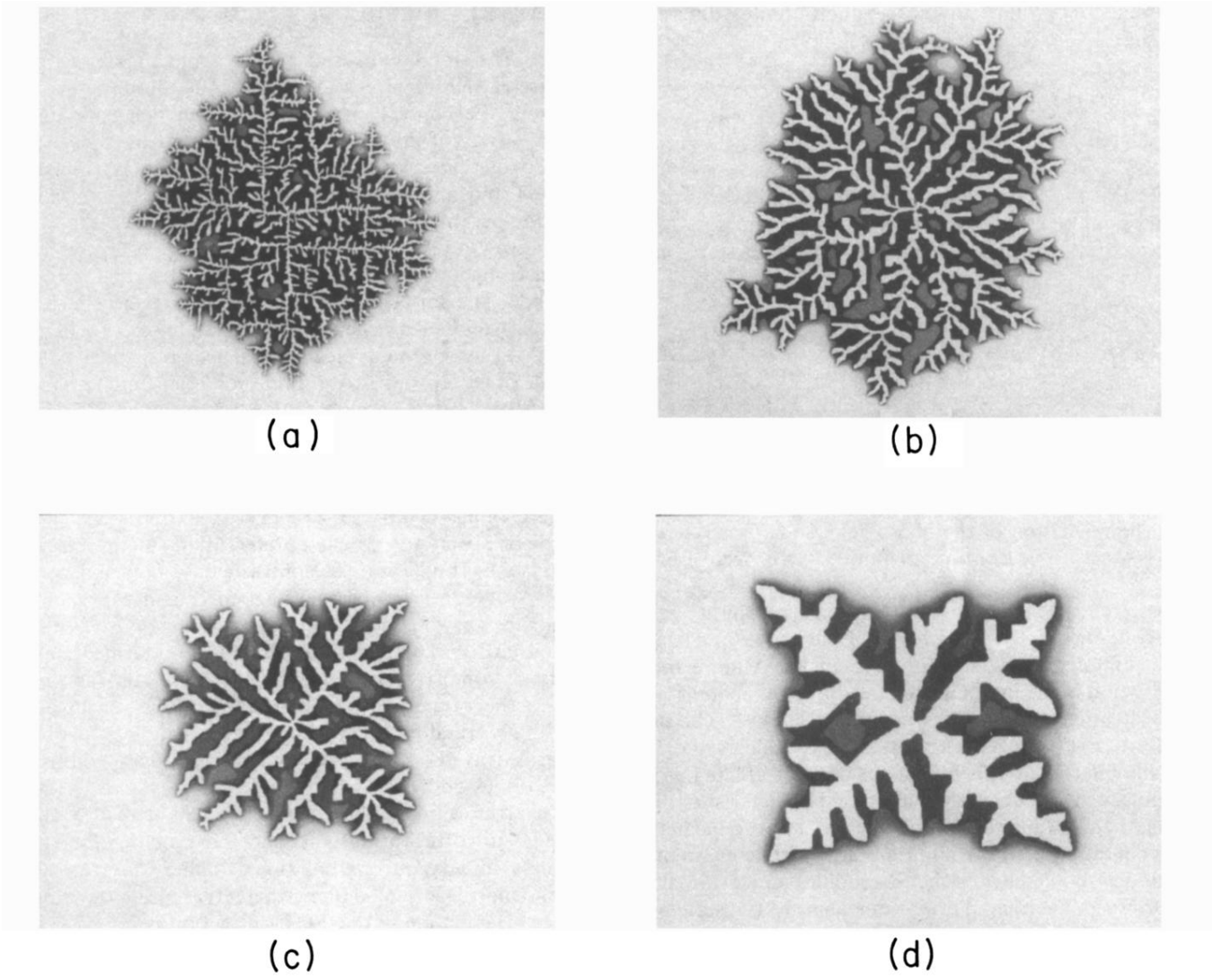

FIG. 2. The morphological transition from axial to diagonal growth. All crystals are grown at $\lambda=0.01$, $\delta=0.2$, but with different Δ. (a) $\Delta=0.15$, the cluster has 85 171 solid particles; (b) $\Delta=0.125$, with 144 522 particles; (c) $\Delta=0.1$, 94 072 particles; and (d) $\Delta=0.05$, 47 305 particles. The scale of picture (d) has been doubled.

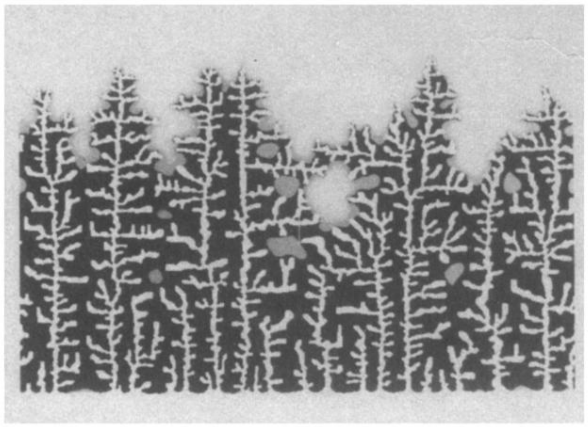

FIG. 7. Sample morphology of the growth from a planar interface. $\Delta=0.1625$, $\lambda=0.01$, and $\delta=0.2$. Periodic boundary conditions are used in the horizontal direction.

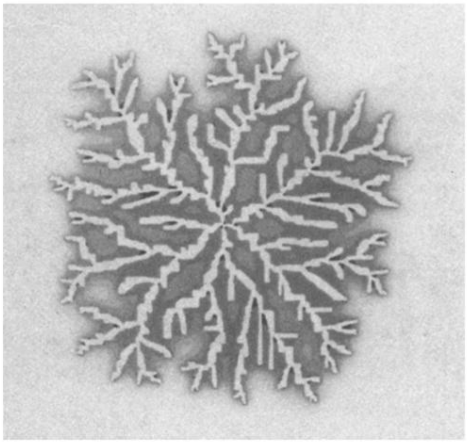

FIG. 9. Crystal grown without noise ($\delta=0$). Other parameters are identical to those of Fig. 2(b).